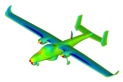

AeroBest 2025
Lisboa, 22–24 April 2025

EXPLOITING POST-BUCKLING NONLINEARITIES FOR GUST LOAD REDUCTION IN HIGH ASPECT RATIO AIRCRAFT WINGS

Pedro Farinha[1*,2], Francesco Toffol[2] and Chiara Bisagni[2]

1: Universidade de Lisboa
Instituto Superior Técnico
Av. Rovisco Pais 1, 1049-001, Lisboa, Portugal
pedro.lourenco.farinha@tecnico.ulisboa.pt, https://tecnico.ulisboa.pt

2: Department of Aerospace Science and Technology
Politecnico di Milano
via la Masa 34, 20156, Milano, Italy
{francesco.toffol,chiara.bisagni}@polimi.it, https://www.polimi.it

Abstract. *The ERC Advanced Grant Project NABUCCO (New Adaptive and BUCkling-driven COmposite aerospace structures) seeks to develop innovative concepts for adaptive and buckling-driven composite structures for next-generation aircraft. By exploiting the buckling phenomena as a design opportunity, the project focuses on utilizing the stiffness redistribution in the post-buckling regime. This study, part of the NABUCCO Project, exploits the structural nonlinearities in the post-buckling regime to mitigate peak loads experienced by high aspect ratio wings, particularly under gust responses. A novel methodology is being developed to incorporate localized nonlinearity introduced by buckling, while maintaining the efficiency of conventional approaches for dynamic load computation. This work focuses on the structural analysis of a wingbox. First, a parametric analysis is conducted to assess the impact of various parameters on the buckling load of a wing section near the root. Based on the results, a new configuration for this section is proposed. Subsequently, a nonlinear analysis is performed on a simplified model to evaluate the stiffness reduction associated with the new configuration. This updated configuration is integrated into the aeroelastic model, and the corresponding results are presented. A structural analysis is carried out to evaluate composite failure, as well as bending and torsion effects on the wing. Preliminary results indicate that the post-buckling response of certain wing components can effectively reduce peak loads caused by gusts, promoting more sustainable aviation practices.*

Keywords: Buckling, post-buckling, gust loads alleviation, structural analysis

Acknowledgements: Funded by the European Union (ERC Advanced Grant, NABUCCO, project number 101053309). Views and opinions expressed are however those of the authors only and do not necessarily reflect those of the European Union or the European Research Council Executive Agency. Neither the European Union nor the granting authority can be held responsible for them. The author Pedro Farinha thanks the Erasmus+ Internship Program for funding this opportunity and Professor Afzal Suleman from Instituto Superior Técnico for supervising this work.

1 INTRODUCTION

With air traffic expected to rise to 25 million flights annually in Europe by 2050, it is pivotal to develop new ways to decrease the impact of aviation on the environment and society. The European Union objectives, defined in the FlightPath2050 document [1], call for a 75% reduction in CO_2 emissions per passenger kilometer, a 90% reduction in nitrogen oxide (NOx) emissions, and a reduction of 65% of the perceived noise.

Advancements in materials, such as the use of high-strength composites, have led to a decrease in weight [2]. Additionally, increasing the wing aspect ratio reduces aerodynamic-induced drag, improving the lift-to-drag ratio and range, but also introduces greater structural flexibility and higher stress levels at the wing root. Reinforcing the wing's internal structure mitigates these issues but increases weight, and reduces fuel efficiency. Moreover, airports and maintenance facilities limit commercial aircraft wingspan [3].

Higher flexibility of the wings poses aeroelastic challenges, where aerodynamic loads cause wing deflection, further altering the loads and possibly leading to catastrophic results [4]. Wind gusts and turbulence increase the Wing Root Bending Moment (WRBM), affecting airframe loads, which can be analyzed using aeroelastic models [5]. Research in Gust Load Alleviation (GLA) techniques has been increasing with passive techniques leveraging structural deformation and active methods using controlled systems to mitigate loads [6].

Various passive load alleviation techniques have been researched. Hahn and Haupt [7] explored the effect of nonlinear behavior of the wing design to trigger downward twist and camber line or profile change. Runkel et al. [8] present a shape adaptation technique for wing structures that enables passive variations in twist. Hahn et al. [9, 10] also suggest a load alleviation concept which incorporates a component inside the wing structure which buckles at a critical load higher than cruise lift leading to a upwards deformation of the trailing edge, resulting in a reduction of the effective angle of attack and a reduction of lift. Ahmadi et al. [11] introduced a new method for the design and optimization of high aspect ratio composite wings that are equipped with passive control devices. while Vaneck et al. [12] invented a stiffness-adaptive wing structure for passive load alleviation which consists of alternating rigid and inflatable spar sections.

Beyond passive load alleviation techniques, numerous active load alleviation approaches have also been developed recently. Toffol and Ricci [13] summarize the work developed within the Clean Sky 2 AIRGREEN2 project, where an innovative wing tip with an additional control surface was developed, achieving between 4 to 17% reduction in WRBM. Stanford [14] performed an optimization of the control surfaces of a high aspect ratio wing for Maneuvre Load Alleviation (MLA) and unsteady GLA.

The ERC Advanced Grant Project NABUCCO (New Adaptive BUCkling-driven COmposite aerospace structures) [15] seeks to develop adaptive buckling-driven structural concepts for the next generation of aircraft. By leveraging buckling as a design opportunity, NABUCCO aims to control structural responses under critical conditions and enable shape variation through non-linear stiffness redistribution induced by the post-buckling regime.

The aim of the research here presented is to reduce WRBM by inducing local buckling at certain locations of the wing, and introduce structural nonlinearity, which can reduce peak loads in cases of gust responses, into the conventional framework for dynamic aeroelastic response calculations. Most current numerical approaches rely on linear aeroelastic

analysis tools, which are inadequate for handling nonlinear stiffness changes induced by buckling. To address this, a novel methodology is being developed that incorporate localized nonlinearity introduced by buckling without significantly increasing computation cost [16, 17].

This paper focuses on the structural analysis of the wingbox of a high aspect ratio wing. The goal is to design a configuration that induces post-buckling in the composite wing skin under critical gust loads. A non-linear analysis is then used to evaluate stiffness redistribution due to buckling, which is subsequently integrated into the aeroelastic framework.

2 NUMERICAL MODEL OF A HIGH ASPECT RATIO WING

The numerical model of the wing analyzed in this study was provided by the Department of Aerospace Science and Technology of the Politecnico di Milano. This model is part of the Ultra High Aspect Ratio Wing Advanced Research and Designs (U-HARWARD) CS2JU founded project [18]. It represents a wingbox similar to that of an Airbus A321, with an aspect ratio (AR) of 15.

This 3D finite element model was generated using the NeoCASS OPtimization Toolbox (NeOPT) [19], an optimization module of the Next generation Conceptual Aero-Structural Sizing Suite (NeoCASS)[20, 21], developed at the Department of Aerospace Engineering at Politecnico di Milano. Using NeOPT, a detailed NASTRAN Finite Element [FE] model of the wingbox was generated from an aeroelastic stick model and subsequently converted to ABAQUS, the solver used for the structural analysis presented in this study.

2.1 Mesh

The FE model consists of composite shell elements (S4R) to represent the skins, while beam elements (B31) are used to model the stringers and spar caps. The ribs are also modeled using shell elements (S4R). The model is divided into five sections along the span, as indicated by the change in skin color shown in Fig. 1. Each section consists of a set of stringers, ribs, and composite skins. Figure 2 provides a close-up view of the first and second sections of the wing, with the upper skin panel removed.

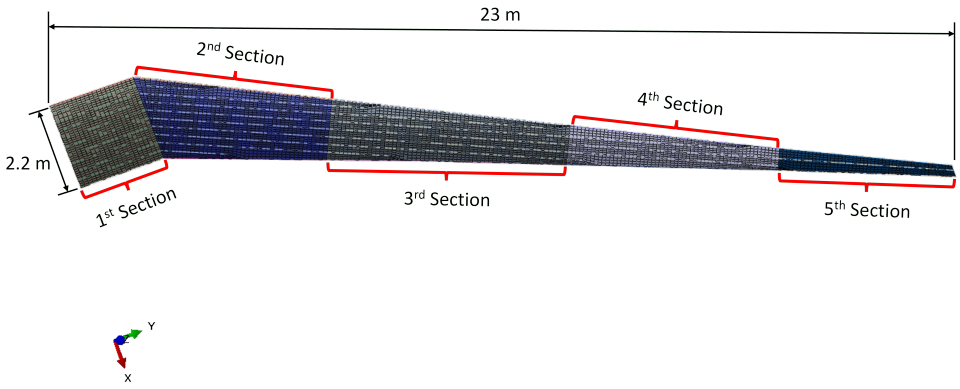

Figure 1: Top view of the whole wingbox.

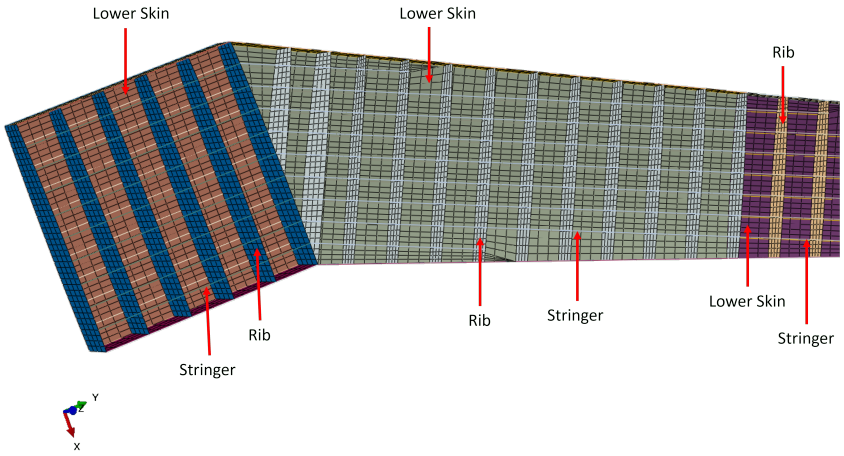

Figure 2: Closeup view of the first and second sections of the wingbox.

2.2 Loads and boundary conditions

The applied loads are derived using NeoCASS's capability to generate a static load set equivalent to a frozen time instant of the dynamic gust. Each load is extracted from the NeoCASS aeroelastic stick model and applied to reference nodes in ABAQUS, which are connected to nodes centered on the ribs' surfaces through kinematic coupling constraints, with all degrees of freedom constrained. The load is then distributed to every node of the rib from this surface node using a coupling constraint. This constraint, shown in yellow in Fig. 3a, enables a weighted distribution of the loads applied at the reference node to the rib nodes, based on a weight factor associated with each coupling node, which depends on its distance from the reference node. Boundary conditions are applied to all nodes of the root rib, constraining all translational degrees of freedom (U1 = U2 = U3 = 0). Figure 3b illustrates the boundary conditions in orange, with forces and moments represented by yellow and purple arrows, respectively. Figure 3 displays only the first and second sections of the wing, however, this method is applied across the entire wingspan.

The loads applied are representative of the most critical case of the wing's response to a gust load, which corresponds to the one that produces the highest wing root bending moment.

(a) Coupling constraints applied on each rib of the model, in yellow.

(b) Loads (arrows) and boundary conditions, in orange, applied on the model.

Figure 3: Closeup views on the coupling constraints, loads, and boundary conditions.

2.3 Materials

The wing skin consists of a carbon fiber composite laminate. Table 1 reports the engineering properties of the laminate. These properties closely resemble those of the

IM7/8552 carbon fiber [22–25]. Table 2 presents the ply strengths of the wing's composite skin. The ribs and stringers are made of an aluminum alloy, with properties listed in Tab. 3 and Tab. 4, respectively.

Table 1: Laminate properties of the wing's skin.

E_1 [MPa]	E_2 [MPa]	ν_{12}	G_{12} [MPa]	G_{13} [MPa]	G_{23} [MPa]	ρ $[kg/m^3]$
161000	11400	0.32	5200	3740	2710	1570

Table 2: Ply strengths of the wing's skin.

X_T [MPa]	X_C [MPa]	Y_T [MPa]	Y_C [MPa]	SL [MPa]
2724	1690	111	264	120

Table 3: Material properties of the ribs.

E [MPa]	ν_{12}	ρ $[kg/m^3]$
72000	0.33	1540

Table 4: Material properties of the stringers.

E [MPa]	G [MPa]	ν_{12}	ρ $[kg/m^3]$
67000	27006.5	0	1570

2.4 Section properties

Table 5 presents the thickness of each wing skin panel, the thickness of the ribs, and the stringer areas for each section.

Table 5: Section properties.

	Section				
	First	Second	Third	Fourth	Fifth
Upper Panel Thickness [mm]	11.67	11.47	14.00	13.47	9.70
Lower Panel Thickness [mm]	11.13	12.20	13.60	12.80	12.80
Ribs Thickness [mm]	12.00	6.00	4.00	3.00	3.00
Upper Stringers Area $[mm^2]$	1840	1940	1630	1120	937
Lower Stringers Area $[mm^2]$	1710	1640	1620	1360	901

All composite wing skin laminates are quasi-isotropic and share the same ply stacking sequence, $[0, 45, -45, 90]_s$. Table 6 presents the thickness distribution for each ply orientation:

Table 6: Thickness by ply orientation.

	Orientation			
	0°	45°	−45°	90°
Thickness (%)	30	30	30	10

2.5 Linear static and buckling analyses

Linear static and buckling eigenvalue analyses were performed on the wing model. Applying the gust load, the linear static analysis yields a maximum vertical displacement at the wing tip of $\Delta_z = 2.040\ m$, and the buckling analysis results in a first eigenvalue, corresponding to the first buckling mode, of $\lambda = 3.0438$. Thus, in the original model, buckling occurs only under load conditions three times higher than those applied. Moreover, buckling is localized in a very small region of the wing, specifically at a stringer interruption.

3 SENSITIVITY STUDY OF THE WING

The results of the linear buckling analysis indicate that the original wing model does not present any buckling with the gust load. A sensitivity study using linear static and buckling analyses provides valuable insight into the structural response to design changes, allowing buckling in some parts of the structure.

3.1 Upper panel skin thickness

The first parameter analyzed is the thickness of the upper panel in the wing's second section, while preserving the thickness distribution shown in Tab. 6.

Results showed that reducing the upper panel skin thickness significantly decreases the first eigenvalue. However, an eigenvalue below 1 is only reached at a 50% reduction, which may lead to issues such as ply failure, ultimately compromising the structure's ability to withstand the applied loads. Furthermore, ABAQUS results indicate that the buckling shape remains confined to a very small area, leading to minimal stiffness reduction in the post-buckling regime.

3.2 Stringers area

The influence of the stringers area in the upper and lower skins of the second wing section on the results was also examined. Reducing the upper panel stringers area resulted in small reduction of the eigenvalue, decreasing by only 14.40% with a 50% decrease in stringers area. Furthermore, the buckling region remained small. However, the maximum vertical displacement at the tip was comparable to that observed when varying the upper skin thickness.

The effect of the lower panel stringer area was negligible, therefore this parameter was excluded from further studies.

3.3 Skin thickness and upper stringers area

Given that varying the upper skin thickness and upper stringer area yielded favorable results, the next step in this sensitivity analysis is to assess the combined effect of modifying both parameters simultaneously.

A greater reduction in the first buckling eigenvalue and a higher maximum vertical displacement was achieved compared to only varying the skin thickness, reaching the post-buckling regime with a 40% decrease in skin thickness and upper stringer area. A higher maximum vertical displacement highlights the role of the upper stringers in preventing bending.

3.4 Number of stringers

In an effort to expand the buckling region, the next step in the sensitivity analysis was to assess the effect of the number of stringers in the wing's second section on the results. Since buckling occurred at the trailing edge, the stringers were progressively removed one by one, starting from the trailing edge and moving toward the leading edge.

Removing the first two stringers near the trailing edge reduces the first buckling eigenvalue by nearly 68%, bringing it below 1. In contrast, removing all remaining stringers results in only a 16% further reduction. The removal of stringers expands the buckling area but confines it between ribs, forming elongated chord-wise buckling zones. Aerodynamically, this is undesirable since buckling near the leading edge disrupts laminar flow. Ideally, buckling should occur near the trailing edge, where upward deflection reduces the effective angle of attack, thereby decreasing lift and alleviating gust loads [10].

3.5 Number of ribs

The influence of rib count on structural behavior was also examined. Initially, the 12^{th} rib was removed, as it is adjacent to the primary buckling zone. Subsequently, the 13^{th} rib was removed, creating a buckling-prone region between adjacent ribs. In the following analyses, two ribs were removed at a time, one from each side of the region. Since loads are applied at the ribs, their removal redistributes the loads to adjacent ribs through distributing coupling constraints. To preserve the load distribution, the outermost ribs of the second section of the wing were retained. ABAQUS results showed that as more ribs were removed, the buckling area expanded, and the eigenvalue dropped significantly, while the tip displacement remained largely unchanged.

A larger buckling area was achieved, demonstrating that rib removal is crucial for this purpose. However, achieving a first buckling eigenvalue close to 0.7 required removing at least 8 ribs, which is too extreme and leads to other structural issues.

3.6 Configuration study

Based on the previous analyses, it was concluded that rib removal is crucial for creating a significant skin area in buckling. Therefore, the 11^{th} and 12^{th} ribs of the model were removed, creating a new section without ribs, hereafter referred to as the *buckling section* as shown in Fig. 4.

A parametric study was conducted on this model, in which the 11^{th} and 12^{th} ribs were removed, all stringers were retained, and the upper panel skin thickness in the *buckling section* was the parametric variable. When the skin thickness was reduced by 50%, the first eigenvalue fell below 1; however, the buckling area remained too small. Therefore, it was necessary to remove stringers and ribs from the model.

After several iterations, two final configurations were developed. In both configurations, the 11^{th} and 12^{th} ribs were removed. In *Configuration 1*, within the *buckling section*, the

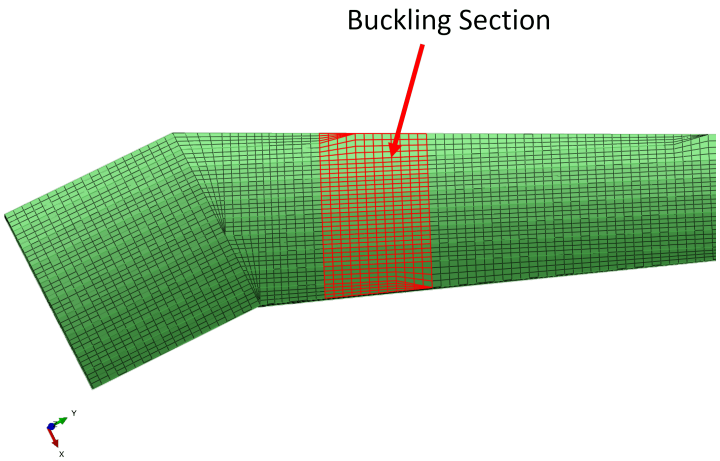

Figure 4: Buckling section region.

two stringers closer to the trailing edge were removed, and the skin thickness was reduced by 10%. In *Configuration 2*, within the *buckling section*, the three stringers closer to the trailing edge were removed, and the skin thickness was increased by 10%. Table 7 presents the results of the linear buckling and static analyses.

Table 7: Linear buckling and linear static analyses results for the two configurations.

Configuration	Eigenvalue	Maximum Tip Vertical Displacement [m]
Configuration 1	0.693	2.056
Configuration 2	0.659	2.052

Both configurations resulted in similar first buckling eigenvalues and tip displacements, differing primarily in the first buckling mode, which influences post-buckling stiffness. Figures 5 and 6 illustrate the results of the linear buckling and static analyses for the two configurations. *Configuration 1* shows a half-wave buckling mode with a larger area than *Configuration 2*.

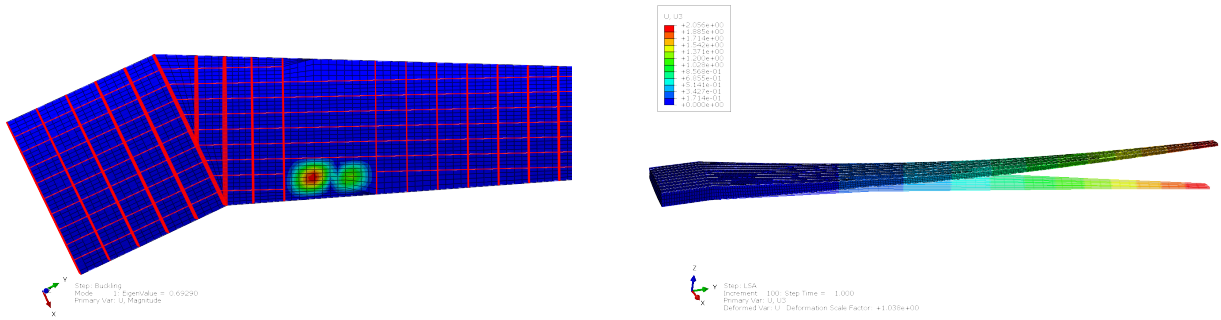

(a) First buckling shape with $\lambda = 0.693$. (b) Deformed shape.

Figure 5: Linear buckling and linear static analyses of Configuration 1.

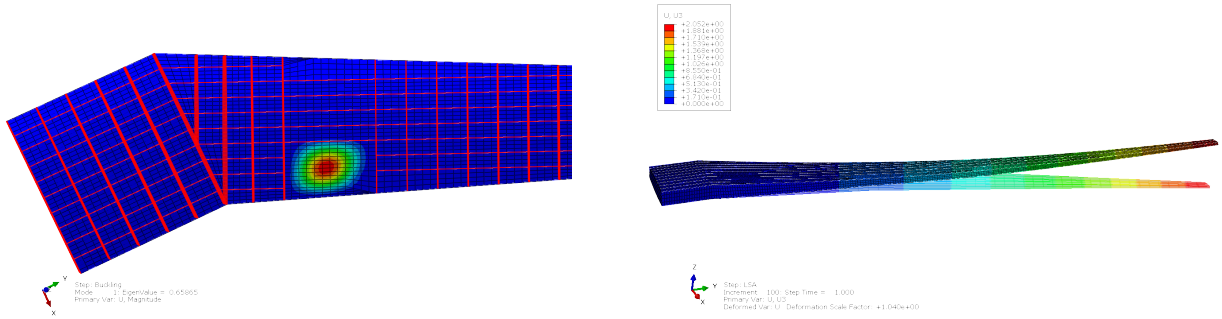

(a) First buckling shape with $\lambda = 0.659$. (b) Deformed shape.

Figure 6: Linear buckling and linear static analyses of Configuration 2.

4 NON-LINEAR ANALYSIS

Both configurations obtained from the parametric study were analyzed in a non-linear analysis. Non-linear analysis allows observation of the skin's displacement behavior over time, enabling the extraction of data from both the pre- and post-buckling regimes.

Although the first buckling eigenvalue of *Configuration 1* was lower than 1, the non-linear analysis revealed that the stiffness variation in post-buckling fiel was minimal, resulting in almost no change in the wing's vertical displacement compared to the linear static solution. The largest change in maximum vertical displacement was only 0.9%. *Configuration 2* exhibited the same behavior, leading to the conclusion that the buckling areas of both configurations were too small to significantly affect the wing's stiffness. Consequently, both configurations were discarded from further studies, and new designs with larger buckling areas were developed.

A new design was developed to achieve a larger buckling region while maintaining a first eigenvalue similar to that of the previous configurations. In this new configuration, the 10^{th}, 11^{th}, 12^{th}, and 13^{th} ribs were removed. Additionally, the four stringers closer to the trailing edge were removed. The thickness of the *buckling section*, now comprising the upper panel skin from the 9^{th} to the 14^{th} rib, was increased by 35%.

However, due to the larger buckling area, it is crucial to ensure that there is no skin failure. Therefore, the first ply-failure criterion, using Tsai-Hill, was evaluated through the non-linear analysis, resulting in a change of the laminate ply orientation to $[-45, 45, 90, 0]_s$, while maintaining the thickness distribution shown in Tab. 6. Figure 7 shows the contour of the maximum Tsai-Hill criterion values across all plies. The peak value obtained is equal to 0.834, ensuring there is no ply failure.

Figure 8 illustrates the buckling shape of this new configuration, with a first mode eigenvalue of $\lambda = 0.63294$.

By comparing the maximum vertical displacements at different spanwise positions, as shown in Tab. 8, both linear and non-linear analyses provide insight into the extent of stiffness reduction due to buckling.

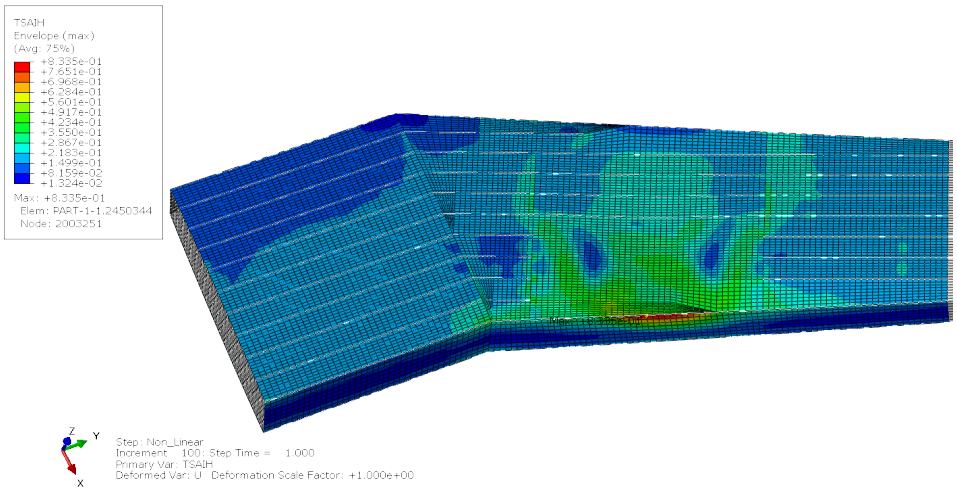

Figure 7: Contour of maximum Tsai-Hill.

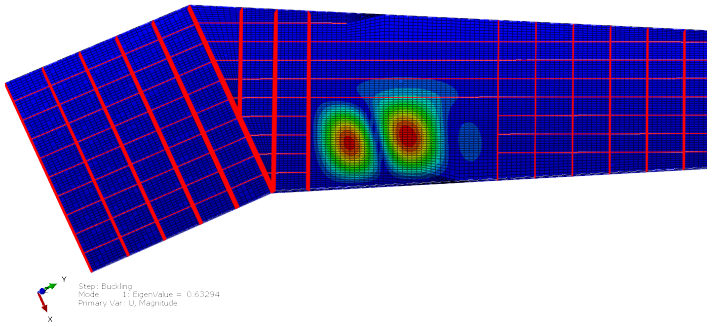

Figure 8: First buckling shape with $\lambda = 0.63294$.

Table 8: Maximum vertical displacement in linear and non-linear analysis.

Node number	Spanwise position [m]	Maximum vertical displacement [m]		Variation [%]
		Linear analysis	Non-linear analysis	
1	1.04	0.00332	0.003340	0.567
2	2.07	0.0109	0.0110	1.58
3	3.91	0.0450	0.0475	5.62
4	5.75	0.101	0.111	9.97
5	6.91	0.155	0.172	10.42
6	8.07	0.224	0.246	9.93
7	9.79	0.354	0.385	8.67
8	11.52	0.519	0.558	7.50
9	13.25	0.718	0.764	6.48
10	14.98	0.952	1.005	5.57
11	16.70	1.217	1.276	4.82
12	18.25	1.477	1.540	4.27
13	19.79	1.755	1.822	3.81
14	21.34	2.038	2.109	3.45

Analysis of the results reveals that nodes near the buckling region experience a more significant stiffness reduction due to the non-linearities of the post-buckling regime, with the maximum vertical displacement increasing by up to 10%.

Figure 9 illustrates the relationship between the total applied force and the vertical displacement of a node at a spanwise position of 6.91 m from the wing root for both linear static and non-linear analyses. The non-linear analysis results begin to diverge from the linear static solution at 55% of the applied gust load, indicating a stiffness reduction and an increase in vertical displacement. This suggests that the skin enters the post-buckling regime at 55% of the gust load whereas the linear buckling analysis predicted a buckling load at 63%. Furthermore, the figure includes linear interpolation equations for both the linear static response and the post-buckling regime in the non-linear analysis. The slopes of these interpolations represent the wing's stiffness at this node allowing the calculation of the stiffness ratio between the pre- and post-buckling regimes. For the node located at a spanwise position of 6.91 m from the wing root, the post-buckling regime results in a 17.4% reduction in stiffness.

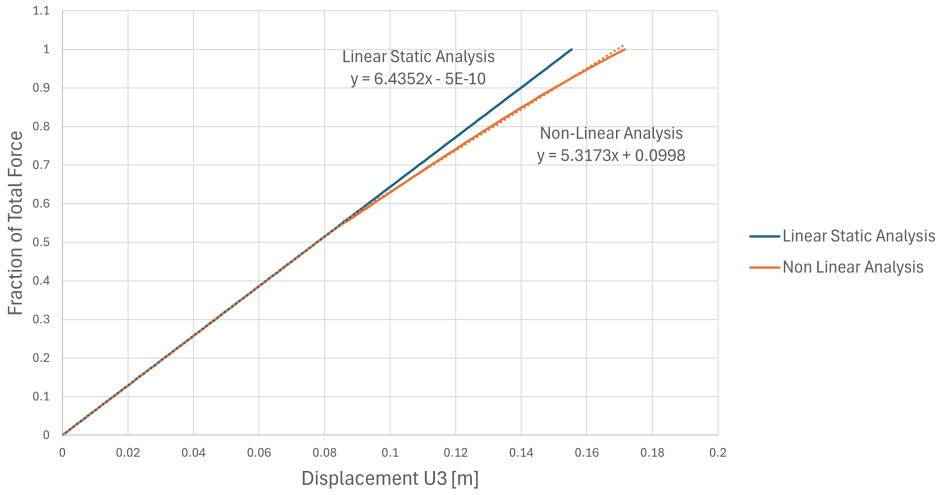

Figure 9: Vertical displacement of a node at a spanwise position of 6.91 m from the wing root in function of total force applied.

5 IMPLEMENTATION INTO AEROELASTIC FRAMEWORK

The post-buckling results obtained from the non-linear analysis can be integrated into the aeroelastic framework to assess the gust load alleviation potential of the proposed configuration, quantified by the reduction in WRBM.

When comparing the non-linear analysis results obtained for the proposed configuration with the linear analysis of the original high aspect ratio wing, an 82% reduction of the buckling load was obtained along with an 11.7% reduction of the post-buckling stiffness. According to the study by Toffol and Bisagni [26], which focuses on the same aircraft, such levels of buckling load and stiffness reduction can lead to an approximate 0.5% decrease in WRBM.

6 CONCLUSIONS

This work presents the structural analysis of a high aspect ratio carbon fiber wing, focusing on leveraging post-buckling behavior in wingbox components to mitigate dynamic peak loads. To achieve this, design modifications were made to induce the wing skin to enter the post-buckling regime.

Buckling analysis carried out in ABAQUS revealed that the buckling load was three times higher than the gust load. A sensitivity study was conducted, to find a configuration with a buckling load lower than the gust load, and a buckling area high enough to produce significant stiffness reduction in the post-buckling regime.

The final configuration achieved a buckling load of approximately 55% of the critical gust load, with the proposed configuration registering an 82% decrease in the buckling load and an 11.7% reduction of the overall stiffness, compared to the original high aspect ratio wing. It was obtained by removing 4 ribs, 4 stringers, and by increasing the skin thickness by 35% and changing the laminate ply sequence to ensure there was no ply failure.

Preliminary results indicate that a WRBM reduction of 0.5% can be obtained with the proposed configuration. For future work, the latest design will be integrated into the aeroelastic stick model framework to assess whether the achieved stiffness reduction effectively mitigates gust loads dynamically. These advancements aim to develop feasible, robust buckling-driven designs for aerospace structures, contributing to structural weight reduction, lower dynamic loading, and improved fuel efficiency.

REFERENCES

[1] European Commission and Directorate-General for Mobility and Transport and Directorate-General for Research and Innovation. *Flightpath 2050 – Europe's vision for aviation – Maintaining global leadership and serving society's needs*. Publications Office, 2011. doi:10.2777/50266.

[2] C. Soutis. Fibre reinforced composites in aircraft construction. *Progress in Aerospace Sciences*, 41(2):143–151, 2005.

[3] F. Afonso, J. Vale, É. Oliveira, F. Lau, and A. Suleman. A review on non-linear aeroelasticity of high aspect-ratio wings. *Progress in Aerospace Sciences*, 89:40–57, 2017.

[4] J. Bussemaker. Wing optimization with active load control. *Master's Thesis, Faculty of Aerospace Engineering, TU Delft, Delft, The Netherlands*, 2018.

[5] D. Balatti, H. Haddad Khodaparast, M. I. Friswell, M. Manolesos, and M. Amoozgar. The effect of folding wingtips on the worst-case gust loads of a simplified aircraft model. *Proceedings of the Institution of Mechanical Engineers, Part G: Journal of Aerospace Engineering*, 236(2):219–237, 2022.

[6] C. L. Bottasso, F. Campagnolo, A. Croce, and C. Tibaldi. Optimization-based study of bend–twist coupled rotor blades for passive and integrated passive/active load alleviation. *Wind Energy*, 16(8):1149–1166, 2013.

[7] D. Hahn and M. Haupt. Exploration of the effect of wing component post-buckling on bending-twist coupling for nonlinear wing twist. *CEAS Aeronautical Journal*, 13 (3):663–676, 2022.

[8] F. Runkel, U. Fasel, G. Molinari, A. F. Arrieta, and P. Ermanni. Wing twisting by elastic instability: A purely passive approach. *Composite Structures*, 206:750–761, 2018.

[9] D. Hahn, M. Haupt, and S. Heimbs. Load alleviation capabilities of wings with nonlinear structural behavior in stationary and dynamic load cases. In *International Forum on Aeroelasticity and Structural Dynamics, IFASD, Madrid, Spain*, pages 642–646, 2022.

[10] D. Hahn, M. Haupt, and S. Heimbs. Passive load alleviation by nonlinear stiffness of airfoil structures. In *AIAA SciTech 2022 Forum*, paper AIAA 2022-0318, 2022.

[11] M. Ahmadi, T. Farsadi, and H. H. Khodaparast. Enhancing gust load alleviation performance in an optimized composite wing using passive wingtip devices: Folding and twist approaches. *Aerospace Science and Technology*, 147:109023, 2024.

[12] T. Vaneck and R. Parks. Wing load alleviation structure. *Patent US8720822*, 2014.

[13] F. Toffol and S. Ricci. Development of an active wingtip for aeroelastic control. *Aerospace*, 10(8):693, 2023.

[14] B. Stanford. Optimal aircraft control surface layouts for maneuver and gust load alleviation. In *AIAA SciTech 2020 Forum*, paper AIAA 2020-0448, 2020.

[15] ERC NABUCCO - New Adaptive and BUCkling-driven COmposite aerospace structures. `https://www.aero.polimi.it/it/progetti-di-ricerca/erc-nabucco-new-adaptive-and-buckling-driven-composite-aerospace-structures`. Accessed: 25-03-2025.

[16] F. Toffol and C. Bisagni. Gust load passive alleviation by means on nonlinear, buckling driven, structural response. In *ICAS Proceedings*. International Council of the Aeronautical Sciences, paper ICAS2024_0147, 2024.

[17] C. Bisagni. Nabucco take-off: Multi-stable panels for an adaptive wing. In *ICAS Proceedings*. International Council of the Aeronautical Sciences, paper ICAS2024_1230, 2024.

[18] U-HARWARD PROJECT. Ultra High Aspect Ratio Wing Advanced Research and Designs. `https://www.u-harward-project.eu/project/`. Accessed: 25-03-2025.

[19] F. Toffol and S. Ricci. Neopt: an optimization suite for the aeroelastic preliminary design. In *18th International Forum on Aeroelasticity and Structural Dynamics (IFASD 2019)*, paper IFASD-2019-020, 2019.

[20] L. Cavagna, S. Ricci, and L. Travaglini. Neocass: an integrated tool for structural sizing, aeroelastic analysis and mdo at conceptual design level. *Progress in Aerospace Sciences*, 47(8):621–635, 2011.

[21] L. Cavagna, S. Ricci, and L. Travaglini. Structural sizing and aeroelastic optimization in aircraft conceptual design using neocass suite. In *13th AIAA/ISSMO Multidisciplinary Analysis Optimization Conference*, paper AIAA 2010-9076, 2010.

[22] HEXCEL. HexPly 8552. `https://www.hexcel.com/user_area/content_media/raw/HexPly_8552_eu_DataSheet(1).pdf`. Accessed: 12-03-2025.

[23] Carbon Fiber Fabric 4 Harness Satin Intermediate Modulus 6k Hexcel IM7 Model #: F-1226-49. `https://compositeenvisions.com/wp-content/uploads/2018/03/F-1226-49-TDS-Hexcel-IM7.pdf`. Accessed: 12-03-2025.

[24] A. E. Lovejoy, S. Scotti, S. Miller, P. Heimann, and S. Miller. Characterization of IM7/8552 thin-ply and hybrid thin-ply composites. In *AIAA SciTech 2019 Forum*, paper AIAA 2019-0773, 2019.

[25] B. P. Justusson, M. T. Molitor, J. S. Iqbal, M. Rassaian, T. M. Ricks, and R. K. Goldberg. Overview of coupon testing of an IM7/8552 composite required to characterize high-energy impact dynamic material models. Technical report, NASA - 2020-220498, 2020.

[26] F. Toffol and C. Bisagni. Passive method for dynamic loads alleviation using structural buckling in a composite wing. In *AIAA SciTech 2025 Forum*, paper AIAA 2025-0425, 2025.